**Steel and Composite Structures**, *Vol. 17, No. 2 (2014) 159-172*
DOI: http://dx.doi.org/10.12989/scs.2014.17.2.159 

# Investigation on low velocity impact on a foam core composite sandwich panel

Zonghong Xie *, Qun Yan [a] and Xiang Li [b]

*School of Astronautics, Northwestern Polytechnical University, Xi'an, China*

(*Received February 02, 2014, Revised May 26, 2014, Accepted June 06, 2014*)

**Abstract.** A finite element model with the consideration of damage initiation and evolution has been developed for the analysis of the dynamic response of a composite sandwich panel subject to low velocity impact. Typical damage modes including fiber breakage, matrix crushing and cracking, delamination and core crushing are considered in this model. Strain-based Hashin failure criteria with stiffness degradation mechanism are used in predicting the initiation and evolution of intra-laminar damage modes by self-developed VUMAT subroutine. Zero-thickness cohesive elements are adopted along the interface regions between the facesheets and the foam core to simulate the initiation and propagation of delamination. A crushable foam core model with volumetric hardening rule is used to simulate the mechanical behavior of foam core material at the plastic state. The time history curves of contact force and the core collapse area are obtained. They all show a good correlation with the experimental data.

**Keywords:** composite sandwich panel; crushable foam core model; low-velocity impact; delamination

## 1. Introduction

Sandwich structure, which is fabricated by attaching two thin but stiff facesheets to a light weight but thick core, is of particular interest and widely used in many applications in aerospace, offshore and sports industries (Park *et al*. 2008, D'Alessandro *et al*. 2014). The concept behind sandwich construction is that the facesheets carry the in-plane tensile and compressive loads, while the light-weight core is to keep the two facesheets apart at a desired distance to provide higher bending stiffness, and also to resist and transmit shear forces to the supporting points (Mostafa *et al*. 2013).

However, the sandwich structure is relatively sensitive to impact loadings due to its poor reinforcement in the thickness direction. A number of research work have shown that an impact load on a sandwich structure can result in the generation of a localized damage which can lead to a significant reductions in its loading-bearing capacity and is hard to be detected (Hazizan and Cantwell 2003, Lacy and Hwang 2003, Anderson and Madenci 2000). At the same time, sandwich structures are prone to impact threats from a wide range of projectiles with various shapes, sizes

*Corresponding author, Professor, E-mail: xzhae@nwpu.edu.cn
[a] Graduate Student, E-mail: yanqun4772@126.com
[b] Ph.D. Student, E-mail: lixianglsx@yahoo.com.cn


http://www.techno-press.org/?journal=scs&subpage=8 ISSN: 1229-9367 (Print), 1598-6233 (Online)

and velocities during the service and maintenance life. Therefore, the damage behaviors under impact load deserve a careful investigation to ensure the reliability and safety of sandwich structures.

## 2. Constitutive models for materials

### 2.1 Intra-laminar damage model

The intra-laminar damage model adopted is based on a Continuum Damage Mechanics (CDM) approach firstly proposd by Kachanov (1987). In the CDM approach, once the certain damage modes initiate in the material, the corresponding material stiffness is degraded to a certain level in order to represent the damage effects. As the damage accumulates, material properties are degraded until the complete failure of the material (Faggiani and Falzon 2010). Damage initiation can be predicted in the numerical analysis by using the damage initiation criteria based on stress or strain. While for composite material analysis, using the strain based criteria is more reasonable because strain fields are directly derived from the deformation field (Rao 2013). In this study, 2D Hashin failure criterion (Hashin 1980) is used to simulate the failure behavior of the facesheets due to impact. For each ply, the fiber is assumed to be parallel and four different failure modes including fiber tensile failure, fiber compressive failure, matrix tensile failure and matrix compressive failure, are considered. The in-plane shear mode alone is not significant and should be considered with the combination of the in-plane tension and compression modes.

The strain based Hashin failure criterion used in current study could be written as following:

(1) If $\varepsilon_{11} \geq 0$, then the fiber tensile failure criterion is

$$r_1^2 = \left(\frac{\varepsilon_{11}}{\varepsilon_{11}^T}\right)^2 + \alpha\left(\frac{\gamma_{12}}{\gamma_{12}^S}\right)^2 \tag{1}$$

(2) If $\varepsilon_{11} < 0$, then the compressive fiber failure criterion is

$$r_1^2 = \left(\frac{\varepsilon_{11}}{\varepsilon_{11}^C}\right)^2 \tag{2}$$

(3) If $\varepsilon_{22} \geq 0$, then the tensile matrix failure criterion is

$$r_2^2 = \left(\frac{\varepsilon_{22}}{\varepsilon_{22}^T}\right)^2 + \left(\frac{\gamma_{12}}{\gamma_{12}^S}\right)^2 \tag{3}$$

(4) If $\varepsilon_{22} < 0$, then the compressive matrix failure criterion is

$$r_2^2 = \left(\frac{\varepsilon_{22}}{2\gamma_{23}^S}\right)^2 + \left[\left(\frac{\varepsilon_{22}^C}{2\gamma_{23}^S}\right)^2 - 1\right]\frac{\varepsilon_{22}}{\varepsilon_{22}^C} + \left(\frac{\gamma_{12}}{\gamma_{12}^S}\right)^2 \tag{4}$$

where: $\varepsilon_{11}^T$ presents the value of $\varepsilon_{11}$ when the longitudinal tensile failure occurs, $\varepsilon_{11}^C$ presents the

value of $\varepsilon_{11}$ when the longitudinal compressive failure occurs, $\varepsilon_{22}^{T}$ presents the value of $\varepsilon_{22}$ when the transverse tensile failure occurs, $\varepsilon_{22}^{C}$ presents the value of $\varepsilon_{22}$ when the transverse compressive failure occurs, $\gamma_{12}^{S}$ presents the value of $\gamma_{12}$ when the longitudinal in-plane shear failure occurs, $\gamma_{23}^{S}$ presents the value of $\gamma_{23}$ when the transverse shear failure occurs, $\alpha$ is a user-specified parameter that determines the contribution of the longitudinal shear stress to fiber tensile failure.

Once any failure occurs, the material may undergo some degree of property loss in the damaged area. The degrees of property loss are strongly dependent on the failure mechanism (Chang 1987). In this study, the continuum damage model presented by Matzenmiller (1995) is used and damage variable $d_i$ is introduced as given in Eq. (5), which acts as a measure of local damage level for a Representative Volume Element (RVE) in composite material. For an undamaged material, $d_i = 0$, while $d_i = 1$ presents a complete failure.

$$d_i = 1 - e^{\left(1-r_i^m\right)/m}, \qquad i = 1, 2 \tag{5}$$

where $m$ is a material-related parameter and is defined as 2 in this study.

Each of the damage variables will affect different components of the effective stress tensor $\tilde{\sigma}$, which can be related to the true stress tensor $\sigma$ via damage matrix $\mathbf{M}$ as

$$\sigma = \mathbf{M} \cdot \tilde{\sigma} \tag{6}$$

$$\tilde{\sigma} = \mathbf{M} : \sigma \tag{7}$$

$$\mathbf{M} = \begin{bmatrix} \dfrac{1}{1-d_1} & & \\ & \dfrac{1}{1-d_2} & \\ & & \dfrac{1}{\sqrt{1-d_1}\sqrt{1-d_2}} \end{bmatrix} \tag{8}$$

Prior to damage initiation, it is assumed that the material is a linear-elastic orthotropic material, where the undamaged material stiffness matrix $\mathbf{C}$ relates the effective stress tensor $\tilde{\sigma}$ to the strain tensor $\varepsilon$ as

$$\tilde{\sigma} = \mathbf{C} \cdot \varepsilon \tag{9}$$

$$\tilde{\sigma} = \mathbf{C} : \varepsilon \tag{10}$$

Then the constitutive law for the damaged material is derived from the principle of energy equivalence as

$$\sigma = \mathbf{C_d} \cdot \varepsilon \tag{11}$$

$$\sigma = \mathbf{C_d} : \varepsilon \tag{12}$$

$$\mathbf{C_d} = \mathbf{M} \cdot \mathbf{C} \tag{13}$$

$$\mathbf{C_d} = \mathbf{M}^{-1} : \mathbf{C} \tag{14}$$

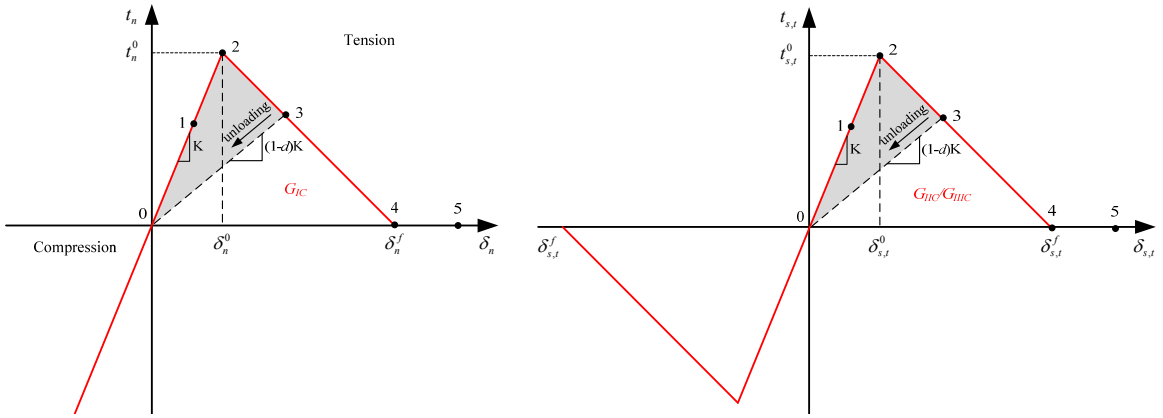


Fig. 1 Inter-laminar cohesive element damage model for pure Mode I and Mode II/III loading

### 2.2 Inter-laminar damage model

Inter-laminar damage, i.e., delamination, is one of the most predominant failure modes in many composite structures, especially when there is no reinforcement in the thickness direction (Camanho 2002, Turon 2007). The simulation of delamination in composite structures is usually divided to delamination initiation and its propagation. The cohesive material model is the most commonly used model in predicting both the onset and propagation of delamination without in advance knowing the location of crack initiation and its propagation direction.

A traction-separation model based on damage mechanics, in conjunction with an initially linear-elastic behavior, is used in the cohesive element model and thus in this study. Fig. 1 illustrates the constitutive behavior of inter-laminar material under pure Mode I and pure Mode II/III loadings.

For pure Mode I or pure Mode II/III loadings, once the interfacial normal or shear tractions reach the inter-laminar tensile strength $t_n^o$ or shear strength $t_{s,t}^o$ respectively, the stiffness is gradually reduced to zero and the area under the traction-displacement curves is the corresponding fracture toughness (Rice 1968). In this way, the onset and final relative displacement could be defined conveniently.

In practical applications of composite structures, delamination is likely to occur under mix-mode loadings. The corresponding softening behavior may occur before any of the traction components involved reaches their respective allowables. Therefore, a mixed-mode criterion with the effect of the interaction of traction components for the onset of delamination is used (Cui *et al*. 1992).

$$\left\{\frac{\langle t_n \rangle}{t_n^0}\right\}^2 + \left\{\frac{t_s}{t_s^0}\right\}^2 + \left\{\frac{t_t}{t_t^0}\right\}^2 = 1 \tag{15}$$

The criteria used to predict delamination propagation under mixed-mode loading conditions are usually established by using fracture toughness and energy release rates. A Benzeggagh-Kenane fracture energy based criterion (Benzeggagh and Kenane 1996) is used here to accurately account for the variation of fracture toughness as a function of mode ratio in composites.

$$G_{IC} + \left(G_{IIC} - G_{IC}\right)\left(\frac{G_{II} + G_{III}}{G}\right)^{\eta} = G_C, \quad \text{with} \quad G = G_I + G_{II} + G_{III} \tag{16}$$

### *2.3 Crushable foam core model*

It is assumed that the rigid closed-cell foam is isotropic. And it should be mentioned that the mechanical properties of a rigid closed-cell foam material is different from those of traditional structural materials, such as steel, mainly due to the plastic compressibility of the foam materials (Rizov 2006).Opposite to solid material, the foams can yield under hydrostatic loading in addition to deviatoric loading. Thus, the yielding criteria for foam materials should include the dependence on the hydrostatic pressure (Deshpande and Fleck 2000).

For the plasticity behavior of foam core material, the yielding surface is an ellipse in the meridional stress plane as shown in Fig. 2 (Yang 2013, Kelly 2012). Two hardening models are available: the volumetric hardening model and the isotropic hardening model. In this study, the volumetric hardening model is adopted and its yielding surface could be defined as

$$f = \sqrt{\sigma_{eq}^2 + \beta^2\left(\sigma_m - \frac{\sigma_c - \sigma_t}{2}\right)^2} - \frac{\beta\left(\sigma_c - \sigma_t\right)}{2} \tag{17}$$

where $\sigma_{eq}$ is the effective stress or von Mises stress defined as Eq. (14) and $\sigma_m$ is the mean stress defined by Eq. (15) (Lubliner 2008, Chakrabarty 2006). $\beta$ is the aspect ratio of the yield ellipse and represents the shape of the yield ellipse in the meridional plane (defined by Eq. (16)). $\sigma_t$ and $\sigma_c$ are the yielding strength in hydrostatic tension and compression respectively. It should be noticed that the yield strength in hydrostatic tension $\sigma_t$ is assumed to remain constant throughout any plastic deformation process in volumetric hardening model.

$$\sigma_{eq} = \sqrt{\frac{1}{2}\left[\left(\sigma_1 - \sigma_2\right)^2 + \left(\sigma_2 - \sigma_3\right)^2 + \left(\sigma_3 - \sigma_1\right)^2\right]} \tag{18}$$

$$\sigma_m = -\frac{1}{3}\left(\sigma_1 + \sigma_2 + \sigma_3\right) \tag{19}$$

$$\beta = \frac{3k}{\sqrt{\left(3k_t + k\right)\left(3 - k\right)}} \tag{20}$$

where $\sigma_i$ ($i$ = 1, 2, 3) are principle stresses, $k$ and $k_t$ are the compression and hydrostatic yield stress ratio defined as

$$k = \sigma_c^Y / \sigma_c^0, \quad \text{with} \quad 0 < k < 3 \tag{21}$$

and

$$k_t = \sigma_t / \sigma_c^0, \quad \text{with} \quad k_t \geq 0 \tag{22}$$

where $\sigma_c^0$ is the initial yielding strength in hydrostatic compression. In this paper, the values of $k$ and $k_t$. are chosen as $k$ = 1.04, $k_t$ = 0.05.

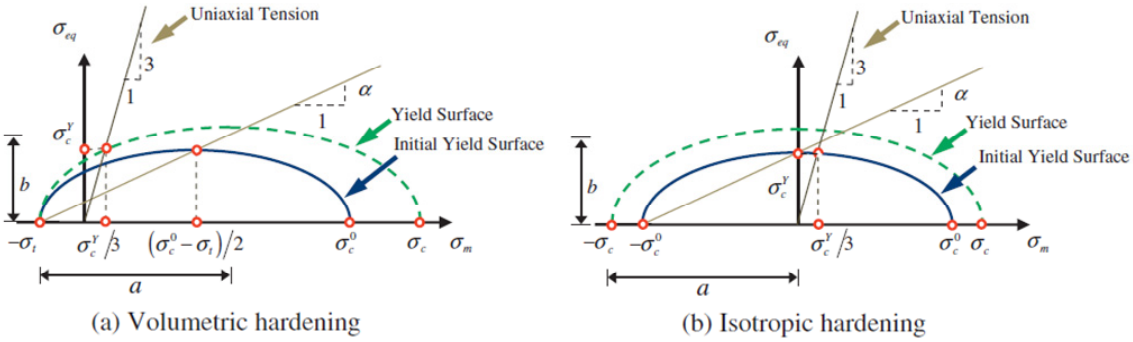


Fig. 2 Yield surface for the volumetric and isotropic hardening in the crushable foam model

Besides this, the flow potential for the volumetric hardening model is chosen as

$$G = \sqrt{\sigma_{eq}^2 + \frac{9}{2}\sigma_m^2} \tag{23}$$

The plastic strain rate is assumed to be

$$\dot{\varepsilon}^{pl} = \dot{\bar{\varepsilon}}^{pl} \frac{\partial G}{\partial \sigma} \tag{24}$$

where $\dot{\bar{\varepsilon}}^{pl}$ is the equivalent plastic strain rate, which is related to the rate of axial plastic strain $\dot{\bar{\varepsilon}}_{axial}^{pl}$ in uniaxial compression by

$$\dot{\bar{\varepsilon}}^{pl} = \sqrt{\frac{2}{3}}\dot{\varepsilon}_{aixal}^{pl} \tag{25}$$

To avoid the current paper from being too lengthy, the hardening methods are not discussed in further details. One can reference ABAQUS Documents (2007) for further information.

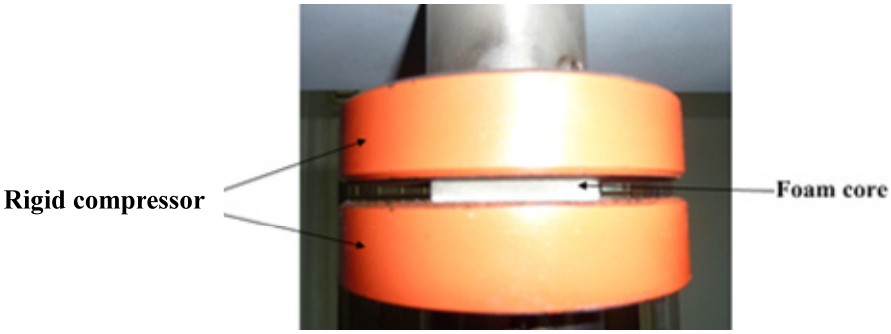


Fig. 3 Flatwise compressive test on foam core material

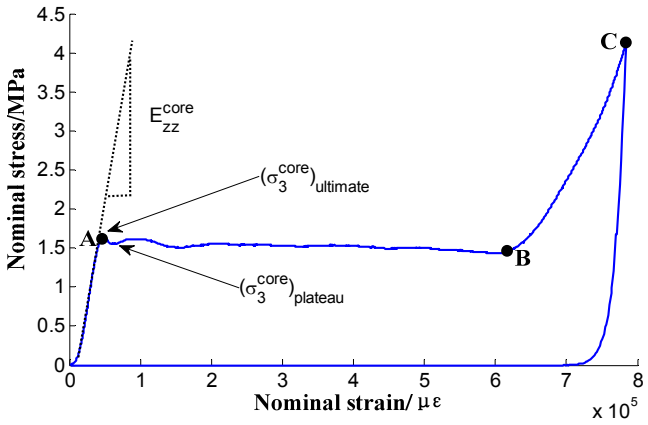


Fig. 4 A typical stress-strain curve from the flatwise compressive test on foam material

## 3. Experimental investigation

### *3.1 Flatwise foam core compressive tests*

The impact loading behavior of foam core sandwich panels strongly depends on the mechanical properties of the core material. According to ASTM C365-5 standard, flatwise compressive tests were carried out to obtain the plastic behavior of the foam material, as shown in Fig. 3. The cubical foam core specimens made by Rohacell 71WF-HT Foam material have the dimensions of 50 mm by 50 mm by 10 mm. During the test, the foam specimens were subjected to a flatwise compressive load with displacement control at a constant loading rate.

A typical stress-strain curve from the flatwise compressive test on foam core is shown in Fig. 4. The nominal stress and strain are defined as

$$\sigma_{nom} = \frac{F}{A} \tag{26}$$

$$\varepsilon_{nom} = \frac{\Delta u}{h} \tag{27}$$

Where $F$ is the compressive force, $A$ is the cross section area of the specimen, $\Delta u$ is the uniaxial displacement and $h$ is the height of the undeformed specimen.

It is clear that the stress-strain curve shows three distinct sections. In section OA, the mechanic behavior of the foam core is linear-elastic. When the stress reaches the limit stress $(\sigma_3^{core})_{ultimate}$ (point A), the core starts crushing under almost constant stress level $(\sigma_3^{core})_{plateau}$ (section AB). The plastic compressibility of the foam core is closely related to the bucking, plastic yielding or brittle crushing of the foam core cell walls. This process progresses at approximately constant stress (plateau stress level) until the cell walls meet and touch to each other. This phenomenon is called foam crushing (Li *et al*. 2000). When all cells are crushed, the stiffness of foam core is increased sharply shown as the lock-up region BC, which corresponds to the compression of a compacted foam.

In plasticity mechanics, true stress and logarithmic strain instead of nominal stress and strain are used. The true stress and logarithmic strain are related to the nominal stress and strain through Eqs. (24) and (25) respectively.

$$\sigma = \sigma_{nom}\left(1+\varepsilon_{nom}\right) \tag{28}$$

$$\varepsilon = \ln\left(1+\varepsilon_{nom}\right) \tag{29}$$

and then the plastic strain of foam core could be calculated by

$$\varepsilon_{pl} = \varepsilon - \frac{\left(\sigma_3^{core}\right)_{ultimate}}{E} \tag{30}$$

where $E$ is Young's Modulus of foam core material. Here from the test result, $(\sigma_3^{core})_{ultimate}$ = 1.7 MPa and $E$ = 105 MPa.

### *3.2 Low velocity impact test*

Drop-weight impact tests (Fig. 5) were performed according to ASTM D7136M-05 test standard. The specimens are sandwich panels composed of two carbon fiber reinforced facesheets and a Foam core. The geometric dimension of the specimens is 150 mm × 100 mm × 7.04 mm. The thickness of foam core is 4 mm. The facesheets are made by T700/BMI. Each facesheet has a quasi- isotropic lay-up of $[45/0/-45/90]_S$ with total thickness of 1.52 mm.

In the test, damage was introduced through a concentrated impact by a 16 mm diameter hemispherical impactor. The impact energy is 10 J with 1.118 m/s corresponding impact velocity. The speccimens were back-supported by a steel plate with a 125 mm × 75 mm square hole as shown in Fig. 6.

The time history of impact force was recorded in the test. One impacted specimen was sectioned along the symmetric plane to study the internal damage state as shown in Fig. 7. It is shown that delamination and core crushing are the two major failure modes for the foam core sandwich panels subject to a low velocity impact.

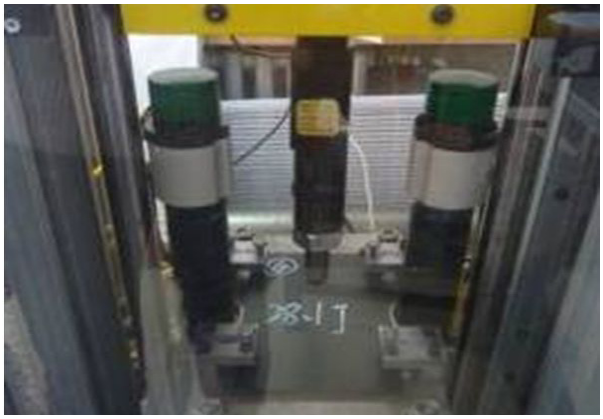

Fig. 5 Drop-weight impact test

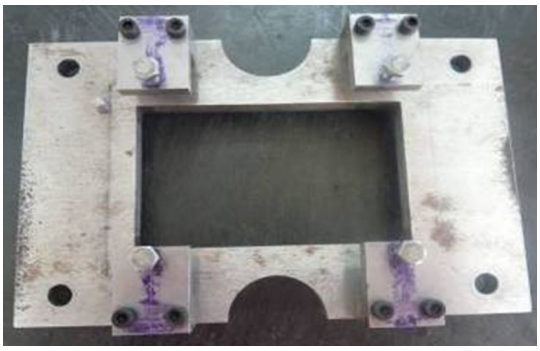

Fig. 6 The support plate used in the impact test

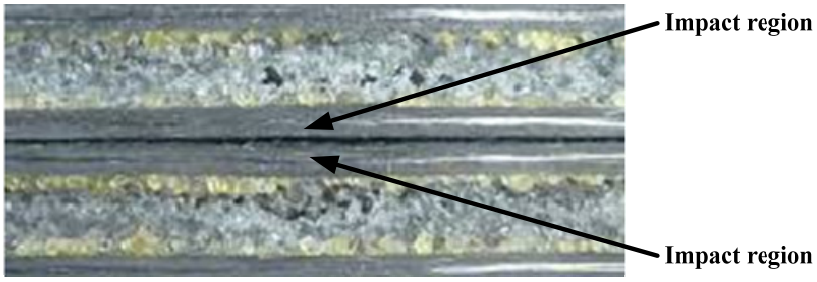


Fig. 7 Damage modes of the specimen subject to a low velocity impact (impact energy: 10 J)

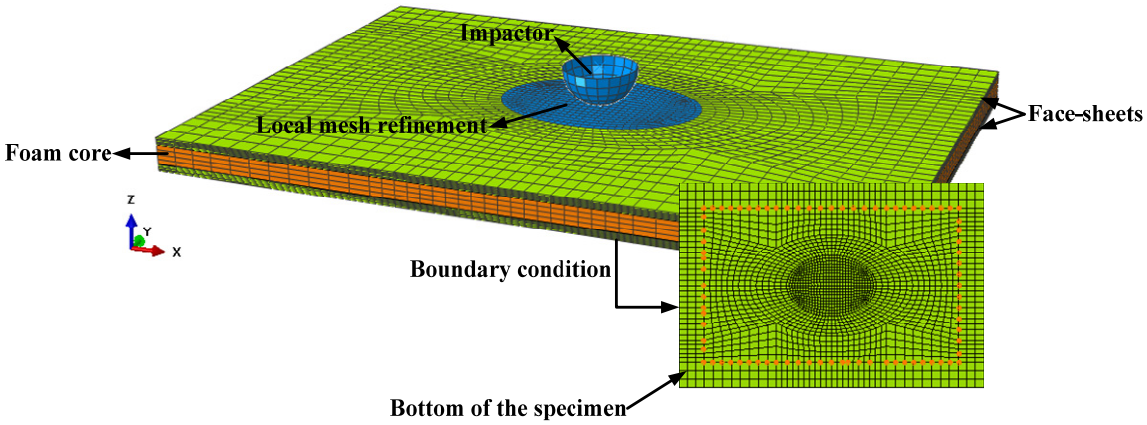


Fig. 8 Details for the finite element model

## 4. Finite element modeling

### *4.1 The modeling*

A numerical finite element model with structural details was generated in ABAQUS to study the impact event and predict the resulting damage modes in the foam core sandwich panel. The

impactor was modeled as a rigid hemispherical shell with 16 mm diameter and a point mass of 16 Kg, just as same as those in the experiment. Fig. 8 shows the finite element model with impact, a refined mesh in impact region and a squared shape support on the bottom of the panel.

All the out-of-plane deformation on the contact lines of the squared support on the bottom side of sandwich panel were set to be zero to represent the edge support in the test. For the impactor, all freedoms except z-direction movement were restricted and its initial velocity was set to be 1.118 m/s, hitting toward the panel.

A self-developed material subroutine VUMAT was used in the analysis with the incorporation of the Hashin failure criteria introduced before to capture the damage initiation as well as the following mechanical properties softening behavior of the facesheet material during the impact process. In addition, Zero-thickness cohesive elements were used along the interfaces between the facesheets and foam core to simulate the initiation and propagation of delamination (or debonding) between the facesheet and the foam core. Crushable foam core model was adopted to simulate the foam core crushing behavior with corresponding parameters obtained from the test.

### *4.2 Element types and mesh*

A total of 43920 solid elements with reduced integration points were used in the finite element analysis. The mesh around the impact zone was refined. Localized stiffness reductions, which occur due to individual elements failure in the analysis, may cause severe deformations in some elements and thus failure in convergence. To avoid this, damage parameters were limited to a maximum value of 0.999 to prevent excessive element distortion. If any elements failed due to fiber tensile failure, the elements were assumed to fail totally and be removed from the model.

Table 1 Material properties of T700/BMI

| Property | Value |
|---|---|
| Longitudinal modulus, $E_{11}$ [GPa] | 125.7 |
| Transverse modulus, $E_{22}$ [GPa] | 10.0 |
| Poisson's ratio, $v_{12}$ | 0.285 |
| Shear modulus, $G_{12}$ [GPa] | 4.58 |
| Longitudinal tensile strength, $X_T$ [MPa] | 2409 |
| Longitudinal tensile failure strain, $\varepsilon_{11}^{T}$ [$\mu\varepsilon$] | 19165 |
| Longitudinal compressive strength, $X_C$ [MPa] | 981 |
| Longitudinal compressive failure strain, $\varepsilon_{11}^{C}$ [$\mu\varepsilon$] | 7804 |
| Transverse tensile strength, $Y_T$ [MPa] | 29.1 |
| Transverse tensile failure strain, $\varepsilon_{22}^{T}$ [$\mu\varepsilon$] | 2910 |
| Transverse compressive strength, $Y_C$ [MPa] | 216 |
| Transverse compressive failure strain, $\varepsilon_{22}^{T}$ [$\mu\varepsilon$] | 21600 |
| Inter-laminar shear strength, $S$ [MPa] | 92 |
| shear failure strain, $\gamma^S$ [$\mu\varepsilon$] | 20087 |
| Density, $\rho$ [Kg/m$^3$] | 1800 |

Table 2 Material properties for cohesive elements on facesheet-core interfaces

| Property | Value |
|---|---|
| Tensile strength, $t_n^o$ [MPa] | 35 |
| Shear strength, $t_{s,t}^o$ [MPa] | 34 |
| Fracture toughness (Mode I), $G_{IC}$ [N/mm] | 0.2 |
| Fracture toughness (Mode II), $G_{IIC}$ [N/mm] | 0.5 |
| Fracture toughness (Mode III), $G_{IIIC}$ [N/mm] | 0.5 |

### *4.3 Material properties*

The facesheets were made by T700/BMI with material properties shown in Table 1. For the zero-thickness cohesive elements, tensile and shear strength and fracture toughness were listed in Table 2.

## 5. Results and discussion

Numerical results from finite element analysis were compared to the test data for the purpose of model validation. The time history of impact force and the damage modes around the impact region were investigated. Delamination initiation and propagation on the interfaces between the facesheet and the foam core were obtained. The core crushing region due to the impact was also obtained.

### *5.1 Time history of impact force and foam core crushing*

The time history curve of impact force is shown in Fig. 9. A good correlation between the experimental data and numerical results was obtained. The maximum impact force from the numerical prediction is 3.619 KN, which is only 2.3% higher than that of the test data of 3.538 KN. A conical shape plastic yielding region in foam core was also obtained as shown in Fig. 10, which is quite similar to the core crushing region observed in the sectioned specimen after impact.

### *5.2 Discussion*

In summary, the finite element model developed in this study can successfully capture the failure process of a foam core sandwich panel under a low velocity impact. It could be quite useful in study the insight details and much more specific information that cannot be directly obtained from the impact test.

According to the numerical results, when the impact force reaches about 400 N, the plastic yielding of foam core begins to occur. When the impact force increases to about 1200 N, fiber breakage failure appears in the upper facesheet, resulting in a slightly drop in the impact force. When the impact force increases to about 2700 N, a large number of fiber breakage failure appear in the upper facesheet and lead to several sudden drops in the impact force. Once the impact force reaches its maximum value around 3600 N, the velocity of the impactor decreases to zero and begins to re-bounce after that. The total process from contact to separation between the impactor

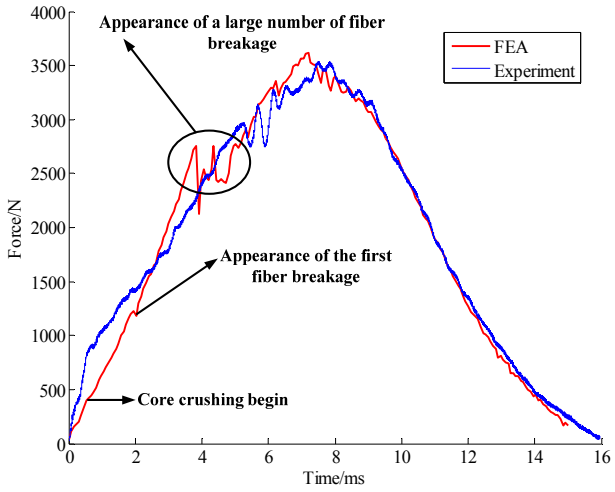


Fig. 9 Time history of impact force (impact energy: 10 J)

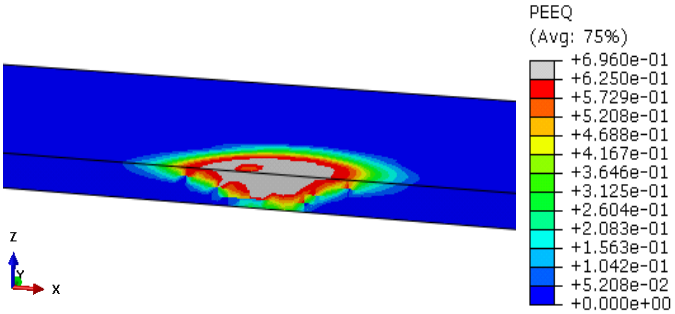


Fig. 10 Foam core crushing region obtained from the finite element model

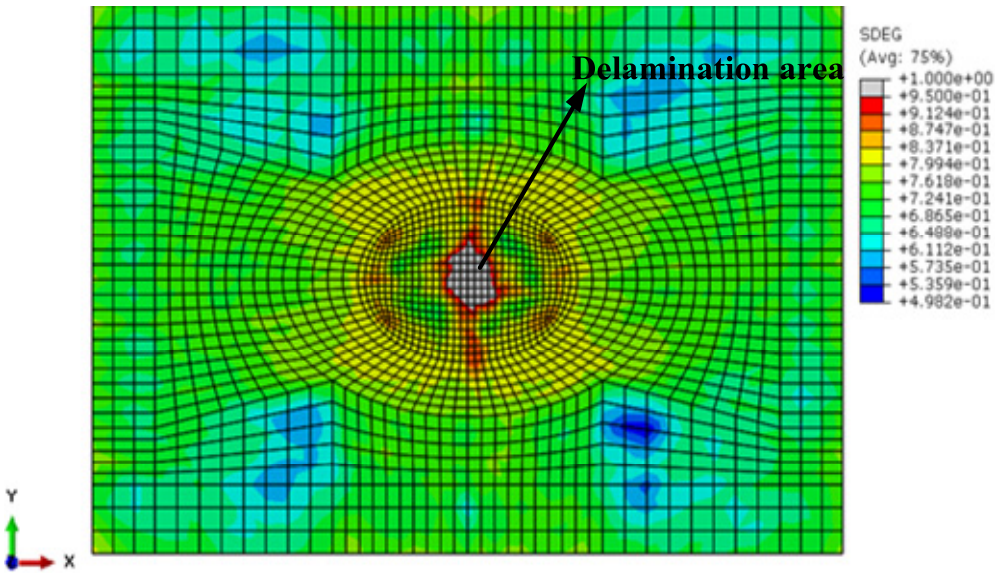


Fig. 11 Delamination on the interface of the upper facesheet and foam core

and the upper facesheet lasts only about 7 to 8 milliseconds.

During the whole impact event, no damage in the lower facesheet was observed. The delamination only occurs on the interface between the upper facesheet and foam core, as shown in Fig. 11.

## 6. Conclusions

This paper presents the work on the implementation of both intralaminar and interlaminar damage models as well as crushable foam model into a detailed finite element model to simulate the low velocity impact event of a foam core sandwich panel. A good correlation between the experimental results and numerical data was obtained in terms of the time history curve of impact load, which validated the numerical model. The numerical results also showed that: (1) intralaminar damage modes, especially fiber breakages, appear and only appear in the upper facesheet around the impact region; (2) a delamination area exists on the interface between the upper-facesheet and the foam core; (3) a significant plastic yielding region in foam core with a conical shape exists under the impact location, which is similar to that observed in the sectioned specimen.

## Acknowledgments

The authors appreciate Beijing Institute of Aeronautical Materials to provide the material properties data and test data for the numerical model validation in this paper.

## References

ABAQUS (2007), "ABAQUS Version 6.7", Dessault Systems; Providence, RI, USA.

Anderson, T. and Madenci, E. (2000), "Experimental investigation of low velocity impact characteristics of sandwich composites", *Compos*. *Struct*., **50**(3), 239-247.

Benzeggagh, M.L. and Kenane, M. (1996), "Measurement of mixed-mode delamination fracture toughness of unidirectional glass/epoxy composites with mixed-mode bending apparatus", *Compos*. *Sci*. *Tech*., **56**(4), 439-449.

Camanho, P.P. (2002), "Mixed-mode decohesion finite elements for the simulation of delamination in composite materials", NASA-Technical Paper 211737, National Aeronautics and Space Agency, USA.

Chakrabarty, J. (2006), *Theory of Plasticity*, Butterworth-Heinemann Ltd., Oxford, UK.

Chang, F.K. (1987), "A progressive damage model for laminated composites containing stress concentrations", *J*. *Compos*. *Mater*., **21**(9), 834-855.

Cui, W., Wisnom, M.R. and Jones, M. (1992), "A comparison of failure criteria to predict delamination of unidirectional Glass/Epoxy specimens waisted through the thickness", *Compos*., **23**(3), 158-166.

D'Alessandro V., Petrone G., Rosa S. and Franco F. (2014), "Modelling of aluminium foam sandwich panels", *Smart Struct*. *Syst*., *Int*. *J*., **13**(4), 615-636.

Deshpande, V.S. and Fleck, N.A. (2000), "Isotropic constitutive models for metallic foams", *JI*. *Mech*. *Phys*. *Solid*., **48**(6), 1253-1283.

Faggiani, A. and Falzon, B.G. (2010), "Predicting low-velocity impact damage on a stiffened composite panel", *Compos*.: *Part A*, **41**(6), 737-749.

Hashin, Z. (1980), "Failure criteria for unidirectional fiber composites", *J*. *Appl*. *Mech*., **47**(2), 329-334.

Hazizan, M.A. and Cantwell, W.J. (2003), "The low velocity impact response of an aluminum honeycomb

sandwich structure", *Compos.*: *Part B*, **34**(8), 679-687.
Kachanov, L.M. (1987), *Introduction to Continuum Damage Mechanics*, Martinus Nijhoff Publishers, Boston, MA, USA.
Kelly, N., McGarry, J.P. (2012), "Experimental and numerical characterization of the elasto-plastic properties of bovine trabecular bone and a trabecular bone analogue", *J. Mech. Behavior Biomed. Mater.*, **9**, 184-197.
Lacy, T.E. and Hwang, Y. (2003), "Numerical modeling of impact-damaged sandwich composites subjected to compression-after-impact loading", *Compos. Struct.*, **61**(1), 115-128.
Li, Q.M., Mines, R.A.W. and Birch, R.S. (2000), "The crush behavior of Rohacell 51WF structural foam", *Int. J. Solid. Struct.*, **37**(43), 6321-6341.
Lubliner, J. (2008), *Plasticity Theory*, Dover Publications Inc., New York, NY, USA.
Matzenmiller, A., Lubliner, J. and Taylor, R.L. (1995), "A constitutive model for anisotropic damage in fiber- composites", *Mech. Mater.*, **20**(2), 125-152.
Mostafa, A., Shankar, K. and Morozov, E.V. (2013), "Insight into the shear behavior of composite sandwich panels with foam core", *Mater. Des.*, **50**, 92-101.
Park, J.H., Ha, S.K., Kang, K.W., Kim, C.W. and Kim, H.S. (2008), "Impact damage resistance of sandwich structures subjected to low velocity impact", *J. Mater. Process. Tech.*, **201**(1), 425-430.
Rao, H., Xu, X.W., Zhu, W.Y. and Zhang, C. (2013), "Numerical simulation of low velocity impact damage on stiffened composite panels", *Acta Materiae Compositae Sinca*, **30**(4), 211-218.
Rice, J.R. (1968), "A path independent integral and the approximate analysis of strain concentration by notches and cracks", *J. Appl. Mech.*, **35**(2), 379-386.
Rizov, V.I. (2006), "Non-linear indentation behavior of foam core sandwich composites – A 2D approach", *Computational materials science*, **35**(2), 107-115.
Turon, A., Davila, C.G., Camanho, P.P. and Costa, J. (2007), "An engineering solution for mesh size effects in the simulation of delamination using cohesive zone models", *Eng. Fracture Mech.*, **74**(10), 1665-1682.
Yang, C., An, Y., Tort, M. and Hodgson, P.D. (2014), "Fabrication, modeling and evaluation of microstructured materials in a digital framework", *Comput. Mater. Sci.*, **81**, 89-97.

*CC*